Polymer 55 (2014) 2543–2551

Contents lists available at ScienceDirect

Polymer

journal homepage: www.elsevier.com/locate/polymer

Role of entanglements and bond scission in high strain-rate deformation of polymer gels

Yelena R. Sliozberg [a,b,*], Robert S. Hoy [c], Randy A. Mrozek [a], Joseph L. Lenhart [a], Jan W. Andzelm [a,**]

[a] U.S. Army Research Laboratory, Aberdeen Proving Ground, MD 21005-5069, USA
[b] Bowhead Science and Technology, LLC, 15163 Dahlgren Rd., King George, VA 22485, USA
[c] Department of Physics, University of South Florida, Tampa, FL 33620-5700, USA

ARTICLE INFO

Article history:
Received 30 January 2014
Received in revised form
10 March 2014
Accepted 24 March 2014
Available online 1 April 2014

Keywords:
Polymer gels
Molecular dynamics simulations
Bond scission

ABSTRACT

A key factor that limits the practical implementation of polymer gels is low gel toughness. Here, we present coarse-grained molecular dynamics simulations of the effects of solvent molecular weight on the toughness of entangled and non-entangled polymer gels in the ballistic impact regime. Our results demonstrate that higher molecular weight solvents enhance gel toughness, and that mechanical properties including strength and toughness can be influenced by bond scission. Further, we find a remarkable two-step gel fracture mechanism on the molecular level: network chains undergo scission first (and well before fracture), followed by scission of solvent chains. For strain rates greater than inverse relaxation time of the solvent, long, highly entangled solvent chains provide fracture resistance even after the network chains break by effectively increasing the number of chains that must be broken as a crack propagates.

1. Introduction

Polymer gels formed by mixing chemically crosslinked polymer networks with solvent molecules exhibit exquisitely tailorable rheological and nonlinear-mechanical properties. Varying the lengths and concentrations of network and solvent chains, as well as chain branching, allows one to vary the gels' linear rheology as well as the fracture toughness [1–3]. However, the practical utility of polymer gels for industrial applications is limited by their low toughness. The need to develop strong and tough gels has intensified interest in understanding the fundamental aspects of their failure mechanisms. Several efforts have been made to enhance mechanical properties of polymer gels including strength, toughness, and durability [4–7]. In particular, recent successful efforts to strengthen gels have employed thermal cycling during processing [4], creation of a double network [5], and synthesizing inorganic-organic hybrid materials [6]. However, many gels remain mechanically fragile. While most gel formulations exploit small molecule solvents such as water or common polymer plasticizers, recent work [7] has demonstrated that both the linear rheological properties and ultimate (fracture) toughness of the gel can be improved by utilizing polymeric solvents rather than small molecules. Polymeric solvents of high molecular weight entangle with the crosslinked polymer network, enhancing the toughness of the gels relative to non-entangled solvents [7]. The mechanical response of these gels ranging from the linear-viscoelastic to fracture regimes arises from the combined contribution of the crosslinked polymer network and the entangled solvent. For example, at strain rates much greater than the inverse relaxation times of the entangled network, the effects of (transient) physical entanglements and (permanent) chemical cross-links are qualitatively similar – both constrain long-range conformational rearrangements of the strands of the polymer network – whereas at lower strain rates, physical entanglements can slip when the network is strained.

Recent computational and experimental research has provided insight into the role of physical entanglements on the mechanical performance of polymer gels with solvent molecular weights large enough to entangle with the polymer network [8]. This work has demonstrated that at moderate to high strain rates, i.e. when the inverse strain rate is smaller or comparable with the reptation time of the solvent, entanglements dominate the stress and the time-

* Corresponding author. U.S. Army Research Laboratory, Aberdeen Proving Ground, MD 21005-5069, USA. Tel.: +1 410 306 0700; fax: +1 410 306 0676.
** Corresponding author. Tel.: +1 410 306 4008; fax: +1 410 306 0676.
E-mail addresses: yelena.r.sliozberg.ctr@mail.mil, ilyapov@gmal.com (Y. R. Sliozberg), jan.w.andzelm.civ@mail.mil (J.W. Andzelm).

http://dx.doi.org/10.1016/j.polymer.2014.03.051
0032-3861/

dependent elastic modulus of polymer gels with high molecular weight. In particular, varying the molecular weight of polymer solvents can be used to tune the rate dependent modulus of polymer gels [8]. However, despite the importance of the gels for industrial, military and biomedical applications [1,9–11] and many theoretical and experimental studies of gel fracture [12–15], there is still comparatively little understanding about the conditions and mechanisms of gel fracture on the molecular level, and it is very difficult for experiments to isolate microscopic fracture mechanisms, e.g. the interplay between chain pullout and scission.

The toughness of polymer is governed by a competition between homogeneous, viscoelastic deformation and various inhomogeneous fracture mechanisms [16]. Since the crack tip zone shows very large deformations in soft solids, accurate description of nonlinear material response is critical for examining gel fracture [17,18]. Even when extreme care is taken, most polymer samples contain various imperfections such as cracks, notches, and extrinsic heterogeneities that concentrate stress and strain and increase local strain rates, all of which localize the *macroscopic* fracture process. Defects such as surface cracks that govern fracture on larger scales are beyond the scope of the present study. However, it is important to understand these local processes in terms of the "intrinsic" mechanical response of flaw-free samples under tensile stress. This intrinsic response is best studied by analytic work as well as numerical simulation. Finite-element methods [19,20] can treat fracture surfaces, but typically make many assumptions about the underlying microscale mechanisms. Molecular simulations can elucidate such mechanisms for a wide variety of relevant parameters such as strand polydispersity, temperature, strain rate, intermonomer interaction strength, chain flexibility, composition, molecular weight, cross-link spacing and entanglement density. This allows isolation of the relative effects of the many competing *molecular-scale* factors present in experiments. In contrast to the wealth of recent simulations of fracture in neat and elastomeric systems in the glassy state [21–30], there have been relatively few simulations of gel fracture [30].

Fracture of polymer gels occurs via two main molecular mechanisms: chain disentanglement or pullout and chain scission. The competition between these depends on the molecular weight of the polymer chains, the number of entanglements along each chain, monomer–scale interactions, chain extension, network connectivity, and the rate of deformation. Sides et al. [30] studied the adhesion between an entangled polymer melt and a polymer-brush-coated substrate over a wide range of temperatures spanning the glass transition. They found that the fracture energy correlates well with the degree of (melt) chain scission. As expected, they found that chain scission increases with increasing melt molecular weight; however, they did not find any substantial difference in pullout/scission mechanisms between uncross-linked melts and cross-linked networks. It should be noted that the strain rates studied by Sides et al. were faster than the inverse Rouse time τ_R^{-1}, where τ_R is the average time required for a chain to crossover from Rouse-like to reptation dynamics [30].

In this work, we focus on the mechanical response of entangled polymer gels at high strain rates (i.e. of order τ_R^{-1}) characteristic of high velocity penetrating events, and particularly on determining the role of entanglements in controlling this response through fracture. We compare this response to that of gels containing short-chain solvents that do not entangle with the network. Our results show a remarkable two-step fracture mechanism for polymer gels containing entangled solvents. Network chains undergo scission first, well before fracture and before scission of solvent chains initiates. This is followed by scission of solvent chains if they are long enough. Our results show that after the network begins to break, long entangled solvent chains provide an additional "backup" fracture resistance by effectively increasing the number of chains that must be broken before a crack can propagate. These findings are in agreement with experimental observations [7] that entangled solvents play a critical role in controlling the nonlinear mechanical response of polymer gels.

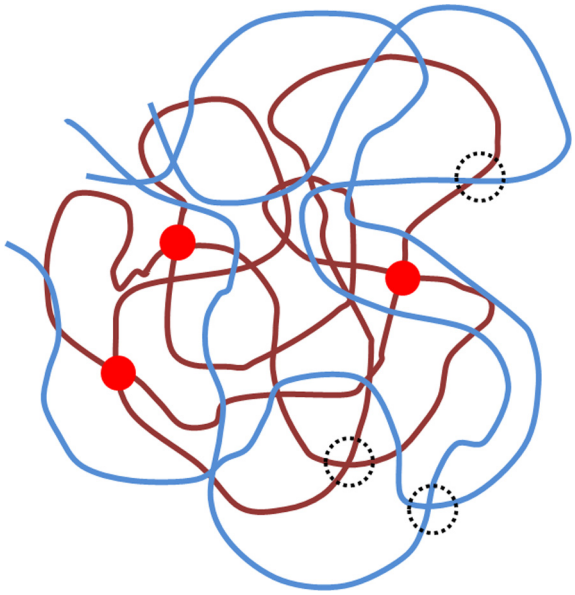

Fig. 1. Schematic representation of the modeled systems. Chains of polymer network and solvent are shown with red and blue colors, respectively. Red dots and dashed circles represent chemical cross-links and physical entanglements, respectively. (For interpretation of the references to color in this figure legend, the reader is referred to the web version of this article.)

2. Model and methods

2.1. Polymer model

We perform molecular dynamics simulations of polymer melts, networks and gels using the Kremer–Grest bead-spring model [31]. Periodic boundary conditions are applied along all three directions of initially cubic simulation cells. All monomers have mass m and the pair interaction between topologically nonconnected monomers is described by the standard truncated Lennard–Jones (LJ) pair potential:

$$U_{LJ}(r) = 4u_0\left[\left(\frac{a}{r}\right)^{12} - \left(\frac{a}{r}\right)^{6} - \left(\frac{a}{r_c}\right)^{12} + \left(\frac{a}{r_c}\right)^{6}\right]. \quad (1)$$

All quantities are expressed in terms of the intermonomer binding energy u_0, monomer diameter a and characteristic time $\tau_{LJ} = \sqrt{ma^2/u_0}$. The LJ potential cutoff is chosen to be $r_c = 2.5a$; this value of r_c produces a glass transition temperature $T_g \sim 0.5u_0/k_B$ [32], i.e. about half the temperature at which our systems are deformed ($T = 1.0u_0/k_B$). Ongoing room-temperature experiments on PDMS gels, which will be reported elsewhere, possess a ratio T_g/T_{room} that is similar to our modeled T_g/T.

Topologically bound monomers interact via the sum of the purely repulsive LJ potential ($r_c = 2^{1/6}a$) or so-called Weeks–Chandler–Andersen U_{WCA} and a quartic potential U_q [23,24]. The quartic potential

$$U_q(r) = (r - \Delta r - b_1)(r - \Delta r - b_2)(r - \Delta r)^2 + U_0, \quad (2)$$

allows bond breaking and prevents unbroken chains from crossing. This potential has a smooth cutoff at $r = \Delta r$ which preserves force

continuity. The parameters in $U_q(r)$ were determined by fitting it to the bond force with the finite extensible nonlinear (FENE) potential at the first zero and the minimum. The potential parameters are $k = 1434.3u_0/a^4$, $b_1 = -0.7589a$, $b_2 = 0.0$, $\Delta r = 1.5a$ and $U_0 = 67.2234u_0$ [24]. The ratio between the forces at which covalent and noncovalent bonds break, about 590, is a reasonable approximation for a coarse-grained polymer model [24], and the model has been used recently to study fracture [21,22,24]. In our simulations, broken bonds are not allowed to reform.

Here, we consider two types of constituents, polymer species A and B. Both polymers are composed of monomers of the same type and have linear topology. Polymer A forms a chemically crosslinked polymer network and polymer B is composed of free solvent chains. Systems composed of both types of polymers (A and B) are polymer gels. We also study pure-network and pure-solvent systems composed respectively only of polymer A or polymer B. In all simulated polymer gels, the volume ratio of network chains is 0.5. Network chains are always fully entangled (as will be shown below), with various arrangements of network–network, solvent–solvent and network-solvent entanglements (Fig. 1).

Physical entanglements represent additional "topological" constraints that contribute to the change of entropy with deformation. Network–network entanglements are permanently trapped during the course of the cross-linking process and affect the chains' configurational entropy to the same degree as cross-links, while network-solvent and solvent–solvent entanglements contribute an entropic term only when they cannot fully relax during deformation. Table 1 lists the lengths of polymer chains for the systems studied here. The total number of coarse-grained particles in all our simulations is $N_{tot} \approx 250{,}000$, with exception of non-crosslinked melt of $N_B = 1000$. For this case, we use a larger system of $N_{tot} \approx 500{,}000$ particles.

2.2. Melt equilibration and network preparation

The simulations are initiated by producing well-equilibrated, uncrosslinked polymer melts. Equilibration of entangled polymers is nontrivial even for coarse-grained systems because of the slow reptation dynamics exhibited by high molecular weight chains. A detailed description of the equilibration algorithm employed in this study is published elsewhere [33]. The main features of this algorithm are: (i) generation of initial chain configurations with large-scale configurations that are as close as possible to equilibrated configurations, and (ii) allowing chains to pass through each other to speed up the polymer dynamics.

After equilibrating the uncrosslinked melts, end-linked polymer networks (polymer A) were prepared by cross-linking the linear chains with cross-linkers containing four-functional groups. Networks are generated by curing well-equilibrated melts of reactant mixture that are composed of M chains of four-arm stars with arm length $N_a = 1$, and $2M$ linear precursor chains of $N_p = 246$. Curing is done in the presence of the nonreactive solvent chains (polymer B). In this stage, the pair interaction between nonbonded particles is described by the excluded volume (Weeks-Chandler-Andersen) potential U_{WCA}, and topologically bound monomers interact according to the standard FENE/Lennard-Jones bonded potential [33]. The network is dynamically formed during NVT simulations with temperature controlled by a Langevin thermostat with damping time 1.0 τ_{LJ}. The end particles of the stars and linear chains react, resulting in a network structure. FENE bonds are formed in the simulation when the separation between ends of a star and a linear chain is less than $1.2a$. To exclude loop formation, the ends of the linear chains are constrained to react with two different stars. To increase the curing rate, attractive LJ interactions ($r_c = 2.5a$) are included between end monomers of the stars and of the linear chains. The curing proceeds until at least 90% of all possible bonds are made (i.e. the cure ratio reaches at least 90%). After network preparation, the LJ potential cutoff is changed to $r_c = 2.5a$ and the systems are equilibrated at zero hydrostatic pressure, yielding an equilibrium monomer number density $\rho = 0.89\ a^{-3}$.

Table 1
Number of coarse-grained particles in a single chain of the network strand N_A and solvent polymer N_B in simulated polymer systems.

N_A	N_B
250	0
250	4
250	500
250	1000
500	0
500	1000
0	500
0	1000

Table 2
The densities of network–network, ρ_e^{AA}, solvent–solvent, ρ_e^{BB}, and network-solvent entanglements, ρ_e^{AB}, and the total entanglement density,ρ_e^{tot}. Densities are given in units of the inverse monomer volume a^{-3}.

N_A	N_B	ρ_e^{tot}	ρ_e^{AA}	ρ_e^{BB}	ρ_e^{AB}
250	0	0.0171	0.0171	0	0
250	4	0.0051	0.0051	0	0
250	500	0.0184	0.0055	0.0051	0.0078
250	1000	0.0179	0.0057	0.0051	0.0071
500	0	0.0178	0.0178	0	0
500	1000	0.0177	0.0053	0.0048	0.0076
0	500	0.0167	0	0.0167	0
0	1000	0.0172	0	0.0172	0

2.3. Deformation

After network preparation, uniaxial-stress tensile deformation is imposed. A constant true strain rate $\dot{e} = 10^{-5}\tau_{LJ}^{-1}$ is applied to the simulation cell, where $e = \ln(\lambda)$ and $\lambda = L_z/L_z^0$. The employed strain rate is much higher than typical experimental strain rates, and corresponds to ballistic impacts. We find, however, that it is still sufficiently slow that segmental contributions to stress are small, and stress–strain curves match the predictions of linear and nonlinear rubber elasticity [34]. A Langevin thermostat with damping time 1.0 τ_{LJ} is used to maintain $T = 1.0$ and a Nose–Hoover barostat with damping time $100\tau_{LJ}$ is used to maintain zero pressure along the transverse directions. The MD time step Δt is $0.0075\tau_L$. All simulations were executed using LAMMPS [35,36]. Finally, an additional simulation at higher strain rate of $\dot{e} = 10^{-4}\tau_{LJ}^{-1}$ is also performed to check the effect of strain rate; the higher rate corresponds to a more viscous regime.

3. Results and discussion

3.1. Topological analysis of the initial configurations

To perform topological analysis of our gels, the numbers of topological entanglements per chain $\langle Z \rangle$ were directly enumerated using the Z1 code [37,38]. Z1's geometrical contour-length reduction algorithm provides the number of interior "kinks" Z corresponding to positions where two primitive paths intersect. Here $Z \propto \langle n_e \rangle$ where n_e is number of rheological entanglements per chain. It has been shown that the number of rheological entanglements,

n_e, is about half the number of topological entanglements, i.e. $\langle Z\rangle \approx 2n_e$ [39].

In Table 2, we report the densities of network–network, ρ_e^{AA}, solvent–solvent, ρ_e^{BB}, and network-solvent entanglements, ρ_e^{AB}, as well as the total entanglement density,ρ_e^{tot}. The entanglement density, which is the number of topological entanglements per unit volume is computed as $\rho_e^k = \langle Z_k\rangle M_k/V$, where M is a number of chains and subscript k corresponds to AA, BB or total. Assuming that all entanglements are binary, the cross-term is found from $\rho_e^{AB} = \rho_e^{tot} - (\rho_e^{AA} + \rho_e^{BB})$.

With the exception of the gel containing low molecular weight solvent, $N_B = 4$, values of ρ_e^{tot} are approximately equal for all systems. These values are close to the expected value$\rho_e^{tot} = 0.0182$ computed from $\rho_e^{tot} = \rho/N_e$, where the topological entanglement length, $N_e \approx 49$, is computed using the "M-kink" estimator [40].

Since all of the gels have the same network fraction $\varphi = 0.5$, the values of the density of trapped entanglements, ρ_e^{AA} are also very similar for all gels, as a result of network chain dilution. This dilution of the network by the polymer solvent leads to a reduction in the number of trapped entanglements according to $\rho_e^{AA} = \rho_e^{bulk}\varphi^\alpha$, where ρ_e^{bulk} is the entanglement density in bulk, φ is the volume fraction of solvent polymer, and α depends on the solvent. We found $\alpha \approx 1.75$ which is within the range $\alpha = 1.7–2.7$ observed in experimental studies [41,42]. Our results are in agreement with those of Mrozek et al. [7]. The authors also observed that solvent molecular weight, M_w does not impact network structure. The gels were formed with solvent of varying M_w, then solvent was extracted and resulted networks exhibited same frequency-dependent rheology [7].

Table 3 shows the number of kinks for the polymer gels and pure network/non-crosslinked polymers. We report $\langle Z_{AA}\rangle$, the number of kinks per A chain created by chains of polymer A, the number of kinks per A and B chain $\langle Z_A\rangle$ and $\langle Z_B\rangle$ from $\langle Z_A\rangle = (\rho_e^{AA} + \rho_e^{AB})V/M_A$ and $\langle Z_B\rangle = (\rho_e^{BB} + \rho_e^{AB})V/M_B$, respectively, where M_A and M_B are respectively the number of chains of polymer A and B. The total number mean of kinks per chain is $\langle Z_{tot}\rangle \geq 5$ for all polymer systems with exception of the "dilute" ($N_B = 4$) gel, indicating these systems should all be in the well-entangled regime, i.e. their mechanical properties are expected to be dominated by entanglements and entanglement relaxation during deformation. The dilute gel has $\langle Z_{tot}\rangle \approx 3$ and is anticipated to show behavior characteristic of the entanglement-onset regime.

From Table 3, one can see that (as expected) increasing solvent chain length does not affect the number of entanglements per network strand, $\langle Z_A\rangle$, but that the number of entanglements per a solvent chain, $\langle Z_B\rangle$ scales linearly with N_B. For example, the two gels $N_A = 250$ $N_B = 500$ and $N_A = 250$ $N_B = 1000$ have approximately equal $\langle Z_A\rangle$, but $\langle Z_B\rangle$ is about twice larger for the gel with $N_B = 1000$. We expect and verify below that increased entanglement between solvent and networks chains improves the toughness of the simulated gels by increasing the number and density of chains that must undergo scission as the crack propagates during incipient fracture.

Table 3
The mean number of kinks,$\langle Z\rangle$ for polymer gels.

N_A	N_B	$\langle Z_{AA}\rangle$	$\langle Z_A\rangle$	$\langle Z_B\rangle$
250	0	5.00	5.00	0
250	4	2.91	2.91	0
250	500	3.06	7.41	14.50
250	1000	3.19	7.12	27.38
500	0	9.99	9.99	0
500	1000	5.98	14.44	27.91
0	500	0	0	9.63
0	1000	0	0	19.29

3.2. Stress-strain response in uniaxial tension

Stress-strain curves for all systems are given in Fig. 2; these are plotted as a function of both the stretch ratio $\lambda = L/L_0$ and the Green–Lagrange strain $g(\lambda) = \lambda^2 - 1/\lambda$. Stress-strain curves are linear in $g(\lambda)$ for small values of λ, showing that our systems display mechanical response consistent with linear rubber elasticity in this regime, i.e. the true stress in uniaxial deformation is $\sigma = G(\lambda^2 - 1/\lambda)$, where G is the shear modulus [34]. For larger λ, curves show nonlinear behavior that arises from entropic depletion of available chain configurations when the inter-crosslink distance becomes comparable to the inter-crosslink chain contour length [43]. All simulated polymers exhibit qualitatively similar behavior: the strain hardening is followed by fracture at the stretch ratio λ_{frac} (strain ε_{frac}) corresponding to maximal stress. For the majority of our systems, stress persists beyond λ_{frac} and does not go to zero during the simulations because the solvent and broken network entanglements are not fully relaxed for the employed strain rate, i.e. "chain pullout" is incomplete. The particle-based molecular dynamics method used in this paper does not allow for performing simulations with lower strain rates due to current computational limitations. Results are truncated at $\lambda = 40$ for all polymer system, since the simulation-cell lateral dimensions become too small at larger strains. The stress–strain curve of the uncrosslinked melt of $N_B = 1000$ is truncated at $\lambda = 50$, since we use a larger simulation cell for this system.

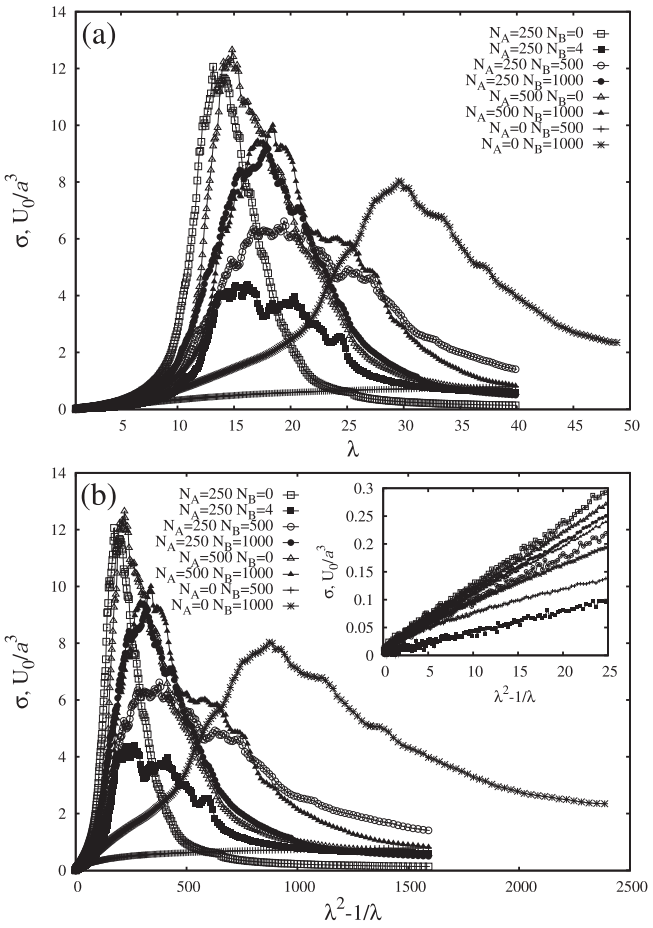

Fig. 2. True stress σ vs. (a) stretch ratio λ, (b) the Green–Lagrange strain $g(\lambda) = \lambda^2 - 1/\lambda$ for uniaxial tension at the true strain rate $\dot{e} = 10^{-5}\tau_{LJ}^{-1}$. The inset to panel (b) shows a zoomed-in region of the same stress–strain curves.

As expected, the pure-network systems show the largest rubber-elastic modulus (steepest rise of stress with strain) since they are the most topologically constrained, i.e. the chemical-crosslink and trapped-entanglement networks are both forced to deform affinely. The initial slopes of the curves vs. the Green–Lagrange strain $g(\lambda)$ are 0.0127 u_0/a^3 and 0.0113 u_0/a^3 for the networks with $N_A = 250$ and $N_A = 500$, respectively. These values are in excellent agreement with the values of the equilibrium modulus (respectively 0.010 u_0/a^3 and 0.009 u_0/a^3 for the networks with $N_A = 250$ and $N_A = 500$) expected from tube theory [44] and measured in many experiments. The equilibrium shear modulus is computed from $G = 4/5\rho k_B T/N_e$ where N_e is the "rheological" entanglement length, i.e. about twice the "topological" entanglement length N_x calculated by Z1 analysis [44]. Alternatively, the equilibrium modulus can be computed from $G = 4/5\rho_c k_B T$, where the total topological constraint density is the sum of the crosslink and entanglement densities, $\rho_c = \rho_x + \rho_e$, and values of ρ_c are equal to 0.0206 a^{-3} and 0.0196 a^{-3} for the networks with $N_A = 250$ and $N_A = 500$, respectively. These systems also exhibit the smallest fracture strain. $\lambda_{frac} \approx 13.5$ and 15.0 for networks with $N_A = 250$ and $N_A = 500$, respectively. Since no chain-scale relaxation can occur, fracture on the macroscale must occur through bond scission. Interestingly, the stress–strain curves of both network are comparable at $\lambda < \lambda_{frac}$ and notably differ at $\lambda > \lambda_{frac}$, where the stress for the network with $N_A = 500$ decreases significantly slower than that for the network with $N_A = 250$. The longer "tail" of stress for the network with $N_A = 500$ is explained by delayed pull-out of longer entangled dangling chains. The mechanical properties of entangled polymer networks at low strain rates are sensitive to defects in the network micro-structure [45,46].

In contrast, the system with no crosslinks (e.g. $N_A = 0$, $N_B = 1000$) is the most ductile and exhibits the largest fracture strain. This is also expected since this system can relax on all scales at sufficiently low strain rates, and fracture can also occur through chain pullout. Finally, we also present results for another entangled ($Z \sim 10$) non-crosslinked melt with shorter chains ($N_A = 0$, $N_B = 500$) that shows very different behavior arising from the fact that the strain rate is less than the inverse Rouse time (cf. Section 3.4) and entanglements can relax significantly over the course of the deformation. This system exhibits viscous flow rather than fracture.

50/50 solvent/network systems show intermediate behavior, with a maximum fracture stress that decreases with decreasing solvent chain length. For example, the most ductile, "softest" system has $N_A = 250$ and $N_B = 4$. This is expected since short solvent chains can both relax conformations and diffuse very quickly; at the studied strain rate, the system behaves essentially like a diluted network with crosslinks and entanglements only between network chains. Consequently, the measured elastic modulus of this gel is also in good agreement with the value of G_e, 0.0042 u_0/a^3 and 0.0037 u_0/a^3 for the measured and expected values, respectively. The elastic moduli of the entangled gels ($N_A = 250$ or 500) do not differ substantially from the expected values; moduli computed from $\rho_c = \rho_e^{tot} + \rho_x$ for two gels with $N_B = 1000$ ($N_A = 250$ and 500) and gels with $N_A = 250$ and $N_B = 500$ are within ~12% of the predictions of rubber elasticity. The stress values after the peak stress at $\lambda_{frac} \approx 18$ correspond to the additional fracture resistance provided by highly entangled solvent chains and dangling ends. This stress resistance is remarkably manifested as a distinct shoulder at $\lambda \approx 24$ at the stress–strain curve of the most entangled gel with $N_A = 500$ and $N_B = 1000$. All simulated networks and gels ($N_A \neq 0$) exhibit a crossover from Gaussian to Langevin (supra-linear) strain hardening around $g(\lambda) = 45–50$, which is compatible with the idea that the latter begins when chain segments between trapped entanglements are stretched to an end-to-end distance about 1/3 of their contour length [43]. The pure-melt systems with $N_B = 1000$ ($N_A = 0$) show a crossover to Langevin strain hardening at a rather larger strain ($g(\lambda) = 150$ *or* $\lambda = 12.3$), consistent with significant large-scale relaxation of chains during the course of the deformation, while those with $N_B = 1000$ actually show behavior that is sublinear in $g(\lambda)$ and reminiscent of transient rubber elasticity (or, more pertinently, of viscous flow) [47] .

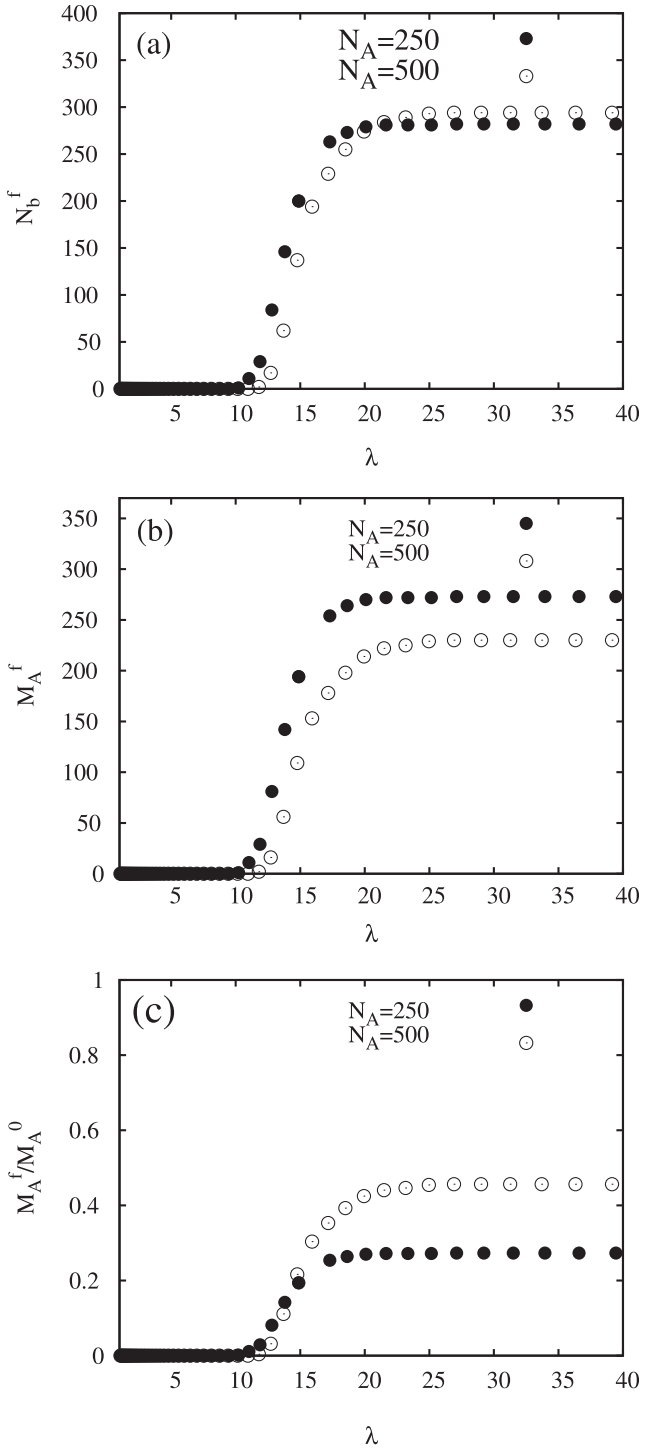

Fig. 3. (a) Total number of broken bonds, N_b^f, (b) number of broken network strands, M_A^f, and (c) number of broken strands normalized by the initial number of strands, M_A^f/M_A^0, as a function of the stretch ratio λ for the pure networks ($N_B = 0$) at a true strain rate $\dot{e} = 10^{-5}\tau_{LJ}^{-1}$.

3.3. Number of broken bonds and toughness

We now move on to a discussion of the micromechanisms of fracture, focusing on bond scission. First we will discuss fracture of two polymer networks ($N_A = 250$, $N_B = 0$ and $N_A = 500$, $N_B = 0$). Our results show that the mechanical responses of these networks are similar (see Fig. 2). Note that the stress tail ($\lambda > \lambda_{frac}$) is larger for the more entangled network with $N_A = 500$ and is a result of high strain rate; at lower strain rates we would obtain sharper fracture for both networks.

For ideal tetra-functional networks with M network chains of N monomers, the total number of bonds is $N_b = (N+1)M$; values of N_b are approximately equal in all our systems ($N_b \approx 250{,}000$). To examine the mechanisms of network fracture, we computed the numbers of broken chains and bonds, as well as how many segments an individual chain breaks into, during the deformation (Figs. 3 and 4). For our chosen covalent bond strength, the onset of bond scission corresponds roughly to the onset of Langevin hardening. Bond scission accelerates rapidly as network integrity progressively breaks down, and reaches a plateau after fracture. We find that the total number of broken bonds during the deformation, N_b^f, is almost equal for both networks, suggesting that both networks have a similar toughness (Fig. 3a). Although the fracture energy depends on the stress associated with bond-breaking, the number of broken bonds is rather small (Fig. 3 (a)), so there are many other important contributors to the stress such as rubber-elastic and viscoelastic effects that could dominate; these will be examined in further detail below.

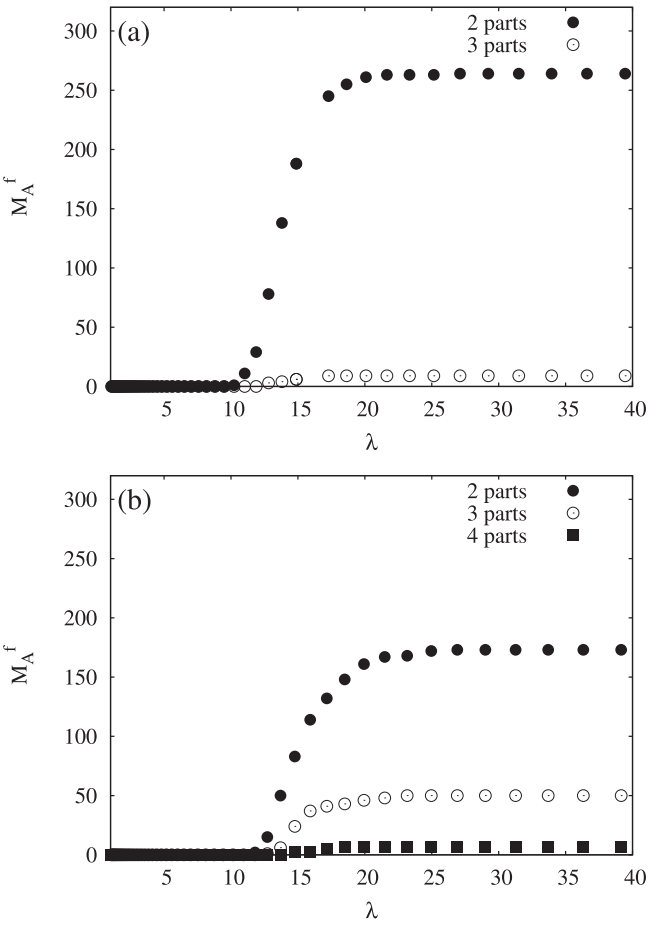

Fig. 4. Number of broken network strands, M_A^f as a function of the stretch ratio λ, for the pure networks ($N_B = 0$) for (a) $N_A = 250$ and (b) $N_B = 500$ at the true strain rate $\dot{e} = 10^{-5}\tau_{LJ}^{-1}$.

The number of broken chains, M_A^f is larger for the network with the shorter strands than for the network with the longer strands (Fig. 3b). Values of M_A^f/M_A^0 are approximately 0.25 and 0.45 for $N_A = 250$ and $N_A = 500$, respectively, where M_A^0 is the initial number of chains. Therefore ~25% and 45% of all chains are broken during the deformation for the networks with $N_A = 250$ and $N_A = 500$, respectively (Fig. 3c). One potential explanation for this somewhat counterintuitive result is that the shorter network chains are weakly entangled and can relax their configurations on the timescales of our simulations, However, this seems to contradict the slightly smaller fracture strain shown in Fig. 2. Another potential explanation involves the number of broken bonds per chain. The equal number of broken bonds and the unequal number of broken chains is explained by the fact that an entangled strand can be broken simultaneously at many places during the tensile deformation. Weakly entangled network chains with $N_A = 250$ typically break into only two parts, but strongly entangled network chains with $N_A = 500$ often break into three or four parts, respectively when two and three bonds simultaneously rupture (Fig. 4). The majority of network chains with $N_A = 500$ rupture into two pieces, and the resulting dangling chains are most likely longer on average than the dangling chains of the network with shorter strands ($N_A = 250$). This leads to a larger stress tail for $\lambda > \lambda_{frac}$ for the network with $N_A = 500$ since pull-out of longer entangled dangling chains requires more work.

Since no chain-scale relaxation can occur for these systems, before chain rupture and fracture on the molecular level occurs through bond scission, we assume that the relevant variable controlling fracture energy is the areal density of broken bonds [30]. We will estimate the threshold fracture energy W_0 with a simple analytic prediction that assumes instantaneous fracture and linear-elastic fracture mechanics. Following Lake and Thomas [48] and including a contribution of the trapped entanglements [49], W_0 is given by multiplying the energy required to rupture a strand of N_{st} monomers, U_{tot}, by the number of chains crossing a unit area in the unstrained state, $\frac{1}{2}\rho_c L$, where L^2 is the average chain end-to end distance, $L \approx \langle R^2 \rangle^{1/2}$. This yields

$$W_0 = \frac{1}{2}\rho_c \left\langle R^2 \right\rangle^{1/2} U_{tot}, \tag{3}$$

ρ_c is the strand density. Under the simplifying assumption that in order to break a bond in a given chain it is necessary to subject all bonds in that same chain to the breaking force [48], $U_{tot} = N_{st}U_0$, where U_0 is the energy required to rupture a monomer unit; for the present model, $U_0 \approx 45u_0$. Assuming that contributions of chemical junctions and entanglements to the elastic network structure are additive, and taking $N_{st} = N_e+1$ for the entangled polymer, the fracture energy is given by

$$W_0 = 0.61 C_\infty^{1/2} l_b \rho_c (N_e + 1)^{1.5} U_0 \tag{4}$$

The numerical factor in Equation (4) is taken from Ref. [48]. Here we have neglected network defects since our cure ratio is larger than 90%. Since $\rho_c = \rho(1/N_e+1/N_c)$ and $N_c >> N_e$, where N_c is the number of monomers between the cross-links for the well-entangled networks, W_0 does not depend strongly on N_c. Thus the molecular-scale fracture energy does not strongly depend on the molecular weight of the network strands. Similar results have been observed in experiments, showing that fracture energy approaches a constant value for networks with strand molecular weight larger than N_e [49]. Note, that Lake and Thomas approach is true only for the “sharp” fracture occurring at the low strain rates

when stress rapidly drops off at λ_{frac}, so the impact of the dangling structures on stress is insignificant. We report values for W_0 in Table 4 and discuss impact of dangling structures on the network toughness in the following section.

Earlier we noted (Fig. 2) that more-entangled systems exhibit larger fracture stresses and smaller fracture strains, and surmised that this arises from the fact that when solvent chains are longer, more chains must be broken as the crack propagates. To confirm this, we examine bond scission in more detail. Fig. 5(a) and (b) show the density of broken backbone bonds N_b^{tot}/V as well as the density of network and solvent broken bonds N_b^{net}/V and N_b^{sol}/V, respectively. For gels, our results show that N_b^{tot}/V increases monotonically with increasing solvent chain length and nearly plateaus for $N_B > 500$. Although N_b^{net}/V of gels of $N_A = 250$ $N_B = 500$ and $N_A = 250$ $N_B = 1000$ are approximately equal (Fig. 5b), the total number of broken bonds, N_b^{tot}/V is larger for the gel dissolved in the longer solvent with $N_B = 1000$ (Figs. 5a and 2). Further, all gels have N_b^{tot}/V lower than values exhibited by pure networks, and N_b^{tot}/V of pure melts is substantially lower than N_b^{tot}/V of the gels. These observations suggest that the trapped entanglements and cross-links dominate the stress associated with bond-breaking. Note that it is reasonable to assume [50] that in all systems except the pure un-crosslinked melts, the number of entanglements before the onset of bond scission is approximately constant during our high strain rate deformation.

Fig. 5 also illustrates an interesting two-step gel fracture mechanism. Network chains undergo scission first, well before fracture. This is followed by scission of solvent chains if they are sufficiently long (Fig. 5b). This implies that after the network chains break, long entangled solvent chains provide additional fracture resistance, thereby effectively increasing the number of chains that must be broken before a crack can propagate. The fact that network strands break first indicates that trapped (network–network) entanglements dominate the initial step of a multistep fracture mechanism of the polymer gels. This phenomenon increases the load borne by the remaining strands, and network-solvent physical crosslinks or entanglements break second. The final entanglements to break are solvent–solvent; this is consistent with the intuitive explanation that solvent chains can relax during deformation, and increasingly so once the first two steps decrease the degree of entanglement trapping. Since the longest considered network strand is $N_A = 500$, the dangling chains, which are produced in the progression of chain rupture, always have length less than 500, and consequently these dangling ends do not rupture during the tensile deformation.

Values of $\langle Z_B \rangle$ taken from Table 3 for the gels of $N_A = 250$ $N_B = 1000$ and $N_A = 500$ $N_B = 1000$ are very close (27.38 and 27.91, respectively).N_b^{tot}/V and the stress responses of these gels are also similar (Figs. 2 and 5a). Fig. 5b shows that solvent and non-crosslinked polymers of 1000 beads undergo chain rupture under deformation. Shorter solvent and non-crosslinked polymers of 500 beads do not rupture (not shown). Our findings are consistent with

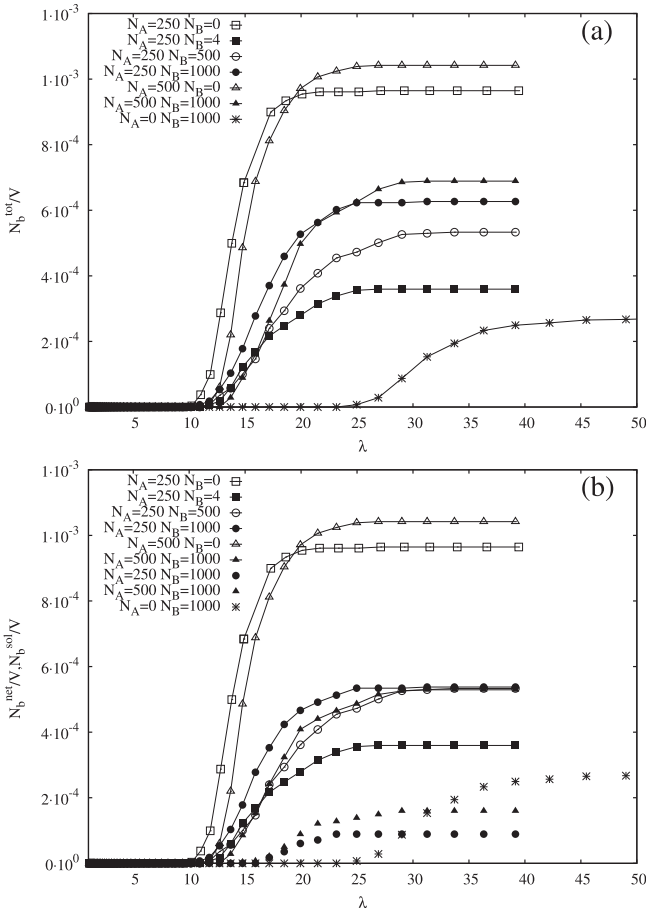

Fig. 5. (a) Total normalized number of broken bonds, N_b^{tot}/V. (b) Normalized number of broken bonds, computed separately for a network and solvent N_b^{net}/V and N_b^{sol}/V shown in connected and unconnected symbols, and symbols, respectively. The strain rate was $\dot{e} = 10^{-5}\tau_{LJ}^{-1}$. The uncross-linked polymer melt ($N_A = 0$ and $N_B = 500$) does not undergo bond rupture (results are not shown).

Table 4
Threshold fracture energy of the polymer networks and gels; theoretical estimates W_0, u_0/a^3 are given by Equation (4) and values W_1 and W_2, u_0/a^3 measured from simulations are given by Equation (6).

N_A	N_B	W_0	W_1	W_2	W_b
250	0	608	570	1470	5.2
250	4	202	359	897	8.9
250	500	597	754	1673	11.1
250	1000	583	880	1707	9.5
500	0	581	687	1963	6.4
500	1000	551	874	1962	10.3

experiments that have demonstrated fracture-like behavior in well-entangled polymer melts of poly(styrene-butadiene) [51] or poly(ethylene oxide) [52] under very rapid step strains; entangled polymeric liquids become solidlike (i.e. behave as nearly elastic rubbers) at such high strain rates.

To illustrate the importance of entanglements to the mechanical properties of the gels, we also evaluated to how many parts an individual network or solvent chain breaks in the tensile deformation for gels. Longer network strands of $N_A = 500$ can break into 3 and 4 pieces even when diluted in solvent, but shorter chains of $N_A = 250$ mostly split into two parts. The polymer solvent of $N_B = 1000$ also splits into two parts, and as mentioned earlier, the polymer solvent of $N_B = 500$ does not rupture at all.

3.4. Relaxation timescale and fracture

Next we relate the results reported above to the underlying relaxation timescales of the systems. The time of simulations from zero to maximum strain is $t_b = \log(\lambda_b)/\dot{e}$ at constant true strain rate $\dot{e} = 10^{-5}\tau_{LJ}^{-1}$. For an elongation-to-break $\lambda_b \approx 15$, the t_b is approximately equal to $3.10^5\tau_{LJ}$. The values of longest viscoelastic relaxation time of the polymeric solvent, i.e. the reptation time t_d, are $7{\cdot}10^5\tau_{LJ}$ and $5{\cdot}10^6\tau_{LJ}$ for $N_B = 500$ and 1000, respectively. We estimated t_d from Ref. [53] as

$$t_d = 0.39N^2(1 + N/N_e), \tau_{LJ}, \quad (5)$$

where the "rheological" entanglement length $N_e = 86$ [40]. Alternatively, t_d could be estimated from eq. (5) by substituting the 0.39 prefactor in eq. (5) with 1.47 as proposed in Refs. [54], yielding values would of $2.5 \cdot 10^6 \tau_{LJ}$ and $1.8 \cdot 10^7 \tau_{LJ}$ for $N_B = 500$ and 1000, respectively. These values are for quiescent systems and are of course shortened in our highly deformed systems via forced reptation, i.e. "chain retraction" [50,55]. Thus t_b is of order the putative reptation time for the shorter ($N_B = 500$) solvent, and nonnegligible compared to it for the longer ($N_B = 1000$) solvent. Further, t_b is larger than the Rouse time, t_R of the shorter solvent and comparable to the Rouse time of the longer solvent, where the t_R are respectively $1.85 \cdot 10^5 \tau_{LJ}$ and $7.4 \cdot 10^5 \tau_{LJ}$ for $N_B = 500$ and 1000. We have estimated t_R from $t_R = N^2/3\pi^2 w\tau_{LJ}$, where $w = k_B T/\zeta C_\infty^{1/2} l_b = 0.025\tau_{LJ} a^{-2}$ and ζ is the onomer friction coefficient [54]. Thus it is possible for fracture to proceed via chain pull-out for our systems. The dangling ends created during chain rupture could also enhance chain pull-out. Note that the relaxation times of these structures are longer than ones of linear unconstrained polymer chains of the same length.

To check whether this occurs, we performed additional simulations for the $N_A = 250$, $N_B = 1000$ polymer gel at a higher strain rate of $\dot{e} = 10^{-4}\tau_{LJ}^{-1}$. At this strain rate, t_b is approximately equal to $t_b \approx 3\ 10^4 \tau_{LJ}$ and $t_b < t_R$. Our results indicate that at $\dot{e} = 10^{-4}\tau_{LJ}^{-1}$, solvent-network entanglements behave similarly to the network–network entanglements; "sliding" of solvent chains is suppressed at this higher strain rate. Consequently, solvent and network chains rupture at the same elongation (Fig. 6). Similar results were observed by Sides et al. [30] in simulations that also had $t_b < t_R$; they did not observe any substantial difference in the chain pullout vs. chain scission competition between pure melts and cross-linked networks.

Thus, our findings suggest that for the chain lengths employed here, at $\dot{e} = 10^{-5}\tau_{LJ}^{-1}$, fracture of polymer gels proceeds via both chain pull-out and chain scission. For the higher strain rate, $\dot{e} = 10^{-4}\tau_{LJ}^{-1}$, fracture proceeds almost exclusively through chain scission.

Comparing our results at the two strain rates, we can see that the maximum at the stress–strain curves corresponds to the onset of bond scission for pure networks (Figs. 2 and 5); stress–strain curves have rather narrow peaks. In contrast, the stress–strain curves of the gels with $N_B > 4$ show some roughness that corresponds to the onset of bond scission, but the stress continues to rise, showing that entangled long solvent chains add fracture resistance.

We estimate the fracture energy on molecular level (fracture toughness) W of the polymer networks and gels from the tensile deformation simulations by numerical integration of the stress–elongation curves:

$$W = \int_1^\lambda \sigma d\lambda h(\lambda), \quad (6)$$

where $h(\lambda)$ is the sample length along the deformation direction. We calculated the local fracture energy by integrating the entire curve, defined as W_2, as well as integrating up to the peak stress occurring at $\lambda = \lambda_{frac}$, defined as W_1. The value of W_2 could be used to estimate the local fracture toughness for the viscous flow at $\lambda > \lambda_{frac}$. Results for the molecular-scale fracture toughnesses W_1 and W_2 and the full fracture toughness normalized by the number of broken bonds, $W_b = W_2/N_b$, are shown in Table 4.

These show the same trends that we observed for the stress associated with bond-breaking; for example, the toughness

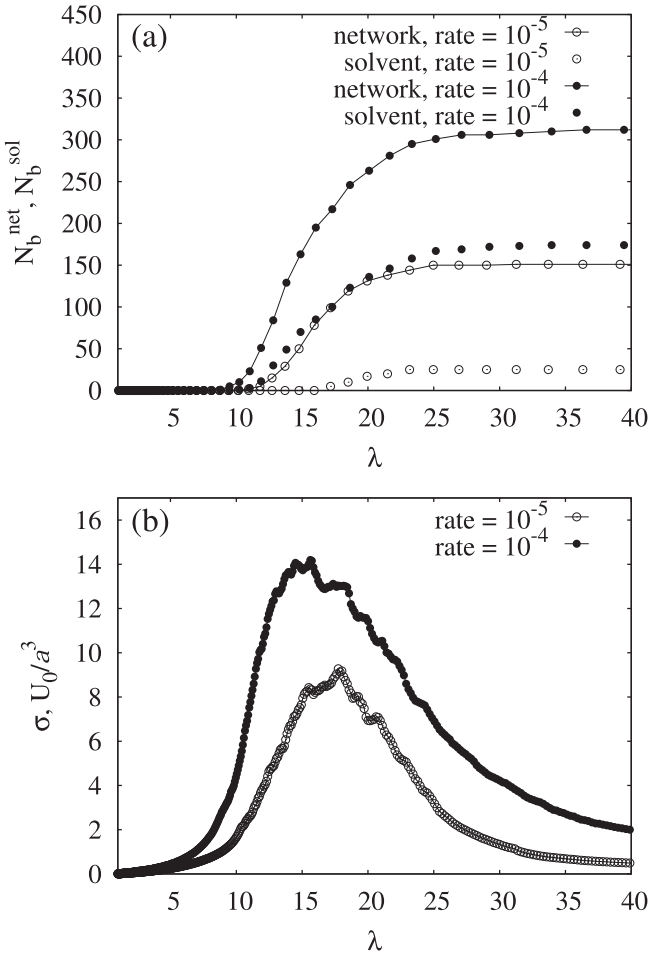

Fig. 6. (a) Total number of broken bonds computed separately for a network and solvent: N_b^{net} and N_b^{sol} for polymer gel with $N_A = 250$ and $N_B = 1000$ for strain rates $\dot{e} = 10^{-4}\tau_{LJ}^{-1}$ and $10^{-5}\tau_{LJ}^{-1}$. (b) True stress σ vs. extension λ.

increases only slowly with the melt strand length for the well-entangled polymer networks. We found that the gels of $N_A = 250$ $N_B = 1000$ and $N_A = 500$ $N_B = 1000$ have very close values of W_1 that correspond to the same number of broken bonds (Fig. 5a). However, the gel with longer network strands ($N_A = 500$ $N_B = 1000$) has markedly higher value of W_2, as can be seen from the noticeable tail of the stress–strain curve.

This can be explained by stress contribution of the longer entangled dangling strands formed by rupture of $N_A = 500$ systems in comparison to those formed by $N_A = 250$ systems. Remarkably, we found that values of W_1 of polymer gels with $N_A = 250$ and $N_B = 500$ and 1000 are respectively ~1.58 and 1.75 times greater than values of W_1 of the pure network with $N_A = 250$, while W_1 of the polymer gel with $N_A = 500$ and $N_B = 1000$ is ~1.40 times greater than the value of W_1 of the corresponding pure network. The total number of broken bonds, N_b^{tot}, is smaller for these gels in comparison to the corresponding pure networks (Fig. 5a). This observation yet again implies that solvent-network entanglements enhance the fracture toughness of gels dissolved in high molecular weight polymers. However, if dangling ends are taken into consideration, the local fracture toughness differs only slightly between entangled polymer gel and entangled networks. W_2 of polymer gels with $N_A = 250$ and $N_B = 500$ and 1000 is ~1.1 times greater than values of W_2 of the pure network with $N_A = 250$, while W_2 of the polymer gel with $N_A = 500$ and $N_B = 1000$ is equal to W_2 of the corresponding pure network. Since the total entangled

densities of the considered entangled polymer gels and networks with exception of gel with $N_A = 250$ $N_B = 4$ are nearly equal, we conclude that the stress at $\lambda > \lambda_{frac}$ is mostly dominated by the entanglement contribution.

Also, we observed that both values of W_1 and W_2 of polymer gels with $N_A = 250$ dissolved in high molecular weight solvent ($N_B = 500$ and 1000) are greater than local fracture toughness of the polymer gel with $N_B = 4$, and W increases with increase of N_B. Analogous results have been observed in experiments by Mrozek et al. [7]; they found that the toughness of PDMS gels diluted in 50% of high-molecular-weight solvent is about 50% higher than, and the toughness of PDMS gels in 50% small-molecule solvents is significantly lower than, the toughness of pure PDMS networks possessing the same network strand length.

The influence of the solvent on the fracture of polymer gels is even more pronounced for the tear energy per broken bond, W_b. W_b increases by ~2.00 times for the entangled polymer solvent $N_B = 500$ and 1000 for the gel with $N_A = 250$ compared to the corresponding pure network. Similarly, W_b of polymer gel with $N_A = 500$ and $N_B = 1000$ is ~1.6 times greater than values of W_b of the corresponding pure network. Table 4 shows that the estimate of the threshold fracture energy obtained from Eq. (4), W_0, is a reasonable estimation for the measured value W_1 for entangled cross-link polymers without solvent. This finding has been confirmed by recent experimental results [56] showing good agreement with the Lake–Thomas model for unentangled gels. However, the Lake–Thomas model cannot make predictions for uncrosslinked systems since it does not include the influence of finite strain rate and non-trapped entanglements. Future molecular dynamics simulations and experiments are necessary to elucidate the molecular pictures behind the macroscopic observations of nonlinear responses of realistic entangled polymers at large fast deformation [57].

4. Conclusion

We performed coarse-grained molecular dynamics simulation showing that the molecular-scale fracture toughness of polymer gels well above their glass transition temperatures strongly depends on chain entanglement in the ballistic regime. Although our results indicate that the trapped entanglements dominate the fracture energy of polymer gels, the solvent-network entanglements play an important role in increasing of the gel toughness by effectively increasing the number of chains that must be broken as the crack propagates. We have shown that polymer gels containing high molecular weight solvents exhibit higher fracture toughness relative to the pure polymer network. This is in dramatic contrast to polymer gels containing low molecular weight solvent that will produce lower fracture toughness relative to the pure polymer network. Our results are in qualitative agreement with experimental observations [7] that entangled solvent substantially increases gel toughness, thereby playing a critical role in controlling the mechanical response of polymer gels. However, they provide a novel insight by relating the stress response of entangled gels to bond scission. We argue that this result is fairly universal since it depends quantitatively but not qualitatively on the activation energy for backbone bond scission. Most importantly, we found a two-step gel fracture mechanism responsible for fracture resistance of the entangled gels at the moderate strain rates: network chains undergo scission first, followed by scission of solvent chains. At higher strain rates, solvent and network chains rupture at the same elongation, leading to single-step gel fracture. In addition, our results suggest that the dangling ends produced in the progression of network chain rupture improve molecular-scale fracture toughness of polymer gels and networks by enhancing chain pull-out.

Acknowledgments

We are grateful to Dr. Tanya L. Chantawansri for productive discussion, and Prof. Martin Kröger for providing the Z1 code.

References

[1] Lenhart JL, Cole PJ, Unal B, Hedden RC. Appl Phys Lett 2007;91:061929.
[2] Mrozek RA, Cole PJ, Cole SM, Schroeder JL, Schneider DA, Hedden RC, et al. J Mater Res 2010;25:1105–17.
[3] Lenhart JL, Cole PJ. J Adhes 2006;82:945–71.
[4] Hassan CM, Peppas NA. Macromolecules 2000;33:2472–9.
[5] Huang M, Furukawa H, Tanaka Y, Nakajima T, Osada Y, Gong JP. Macromolecules 2007;40:6658–64.
[6] Haraguchi K, Takehisa T. Adv Mater 2002;14:1120–4.
[7] Mrozek RA, Cole PJ, Otim KJ, Shull KR, Lenhart JL. Polymer 2011;52:3422–30.
[8] Sliozberg YR, Mrozek RA, Schieber JD, Kröger M, Lenhart JL, Andzelm JW. Polymer 2013;54:2555–64.
[9] Ozkan S, Gillece TW, Senak L, Moore DJ. Int J Cosmet Sci 2012;34:193–201.
[10] Rutkevicius M, Munusami SK, Watson Z, Field AD, Salt M, Stoyanov SD, et al. Mater Res Bull 2012;47:980–6.
[11] Xu H, Wu J, Chu CC, Shuler ML. Biomed Microdevices 2012;14:409–18.
[12] Gong JP. Soft Matter 2010;6:2583–90.
[13] Brown HR. Macromolecules 2007;40:3815–8.
[14] Brown HR, Creton C, Hui C-Y, Jo WH, Kramer EJ, Suematsu K, et al. Molecular simulation/fracture/gel theory (advances in polymer science). Wiley; 1980.
[15] Chaudhury MK. J Phys Chem B 1999;103:6562–6.
[16] Argon AS, Cohen RE. Polymer 2003;44:6013–32.
[17] Hui CY, Jagota A, Bennison SJ, Londono JD. Proc R Soc Lond A 2003;459:1489–516.
[18] Tanaka Y, Fukao K, Miyamoto Y. Eur J Phys E 2000;3:395–401.
[19] Buxton GA, Balazs AC. Macromolecules 2005;38:488–500.
[20] Socrate S, Boyce MC, Lazzeri A. Mech Mater 2001;33:155–75.
[21] Rottler J, Robbins MO. Phys Rev E 2003;68:011801.
[22] Mukherji D, Abrams CF. Phys Rev E 2009;79:061802.
[23] Stevens MJ. Macromolecules 2001;34:1411–5.
[24] Tsige M, Stevens MJ. Macromolecules 2004;37:630–7.
[25] Tsige M, Lorentz CD, Stevens MJ. Macromolecules 2004;37:8466–72.
[26] Rottler J, Robbins MO. Phys Rev Lett 2002;89:148304.
[27] Rottler J, Robbins MO. Phys Rev Lett 2002;89:195501.
[28] Mukherji D, Abrams CF. Phys Rev E 2009;78:050801.
[29] Sides SW, Grest GS, Stevens MJ, Plimpton SJ. J Polym Sci Part B Polym 2004;42:199–208.
[30] Sides SW, Grest GS, Stevens MJ. Macromolecules 2002;35:566–73.
[31] Kremer K, Grest GS. J Phys Condens Matter 1990;2:SA295–8.
[32] Bennemann C, Paul W, Binder K, Dűnweg B. Phys Rev E 1998;57:843.
[33] Sliozberg YR, Andzelm JW. Chem Phys Lett 2012;523:139–43.
[34] Treloar LRG. Physics of rubber elasticity. Oxford University Press; 1975.
[35] http://lammps.sandia.gov.
[36] Plimpton SJ. Comp Phys 1995;117:1–19.
[37] Kröger M. Comput Phys Commun 2005;168:209–32.
[38] Karayiannis NC, Kröger M. Int J Mol Sci 2009;10:5054–89.
[39] Everaers R. Phys Rev E 2012;86:022801.
[40] Hoy RS, Foteinopoulou K, Kröger M. Phys Rev E 2009;80:031803.
[41] Laurer JH, Mulling JF, Khan SA, Spontak RJ, Bukovnik R. J Polym Sci Part B Polym 1998;36:2379–91.
[42] Laurer JH, Khan SA, Spontak RJ, Satkowski MM, Grothaus JT, Smith SD, et al. Langmuir 1999;15:7947–55.
[43] Arruda EM, Boyce MC. J Mech Phys Solids 1993;41:389–412.
[44] Doi M, Edwards SF. Oxford, England: Clarendon Press; 1986.
[45] Jensen MK, Khaliullin R, Schieber JD. Rheol Acta 2012;51:21–35.
[46] Sliozberg YR, Chantawansri TL. J Chem Phys 2013;139:194904.
[47] Ferry JD. Viscoelastic properties of polymers. Wiley; 1980.
[48] Lake GF, Thomas AG. Proc R Soc Lond Ser A 1967;300:108–19.
[49] Mazich KA, Samus MA. Macromolecules 1990;23:2478–83.
[50] Hou JX, Svaneborg C, Everaers R, Grest GS. Phys Rev Lett 2010;105:068301.
[51] Boukany PE, Wang S-Q, Wang X. Macromolecules 2009;42:6261–9.
[52] Fang Y, Wang G, Tian N, Wang X, Zhu X, Lin P, et al. J Rheol 2011;55:939–49.
[53] Kröger M, Hess S. Phys Rev Lett 2000;85:1128–31.
[54] Pütz M, Kremer K, Grest GS. Europhys Lett 2000;49:735–41.
[55] McLeish TCB. Adv Phys 2002;51:1379–527.
[56] Akagi Y, Sakurai H, Gong JP, Chung U, Sakai T. J Chem Phys 2013;139:144905.
[57] Wang S-Q, Wang Y, Cheng S, Li S, Zhu S, Sun H. Macromolecules 2013;46:3147–59.